Back to Session Subjects

ANALYTICAL EVALUATION OF PERFORMANCE ENHANCEMENT OF AN ACTUATED TRAILING EDGE FLAP USING THE COUPLED ROTOR-FUSELAGE MODEL

Dr Wayland Chan
Principal Engineer
(Rotor Technology)

Alan Brocklehurst
Principal Engineer
(Rotor Aeromechanics)

Rotor Systems Group
GKN Westland Helicopters Limited
Yeovil Somerset England

Abstract[1]

An analytical evaluation of the performance enhancement due to a servo-actuated trailing edge flap was carried out using the Coupled Rotor-Fuselage Model (CRFM). The performance enhancement from a trailing edge flap is achieved by introducing effective camber around the azimuth for a nominal aerofoil. An investigation on the best combination of flap parameters, namely the span, position, chord and deflection was carried out in order to identify an optimal configuration within given design constraints. The effects on vibratory control loads over a range of speed for a flap of 10% span, 20% chord, actuated at once per rev has expanded the retreating blade envelope for a Lynx aircraft by some 20kts. The flap hinge load was also examined and it was found not to be excessive. It was also confirmed that an actuated trailing edge flap does not have adverse effect on the pilot's control inputs to trim to a particular flight condition. This paper will discuss the aerodynamic enhancements derived from the application of the trailing edge flap and present conclusions drawn from this study.

Abbreviations and Notations

c	Nominal blade chord;
c_F	Trailing edge flap chord (normalised);
C_L	Lift coefficient;
C_D	Drag coefficient;
C_M	Pitching moment coefficient;
C_{M0}	Moment coefficient at zero angle of attack;
f_c	Correlation factor for an aerofoil;
α_0	Zero lift angle (deg);
θ	Transformation parameter;
δ	Trailing edge flap deflection angle (deg);
α	Blade incidence (deg);
μ	Advance ratio;
BERP	British Experimental Rotor Programme;
CRFM	Coupled Rotor-Fuselage Model;
PEF	Performance Enhancement Flap;
TAS	True airspeed (knots);
CL_{VIB}	Vibratory (half peak-to-peak) control load (lbf);
1R	Once per rev;
Ω	Rotor speed (rad/s);

1. Introduction

An aerofoil designed for use on a helicopter rotor must satisfy the requirements of high lift at low Mach number and low drag at high Mach number. Also at moderate Mach number, e.g. around the fore and aft sectors of the rotor disc or in hovering flight, a good lift/drag ratio is required. A cambered aerofoil may be used to improve performance at high incidence and at low to moderate Mach numbers, but the associated pitching moment on the advancing blade is limiting. An aerofoil, which can change the blade characteristics to suit the varying condition around the azimuth will clearly improve in performance and indeed counter unwanted vibration and impulsive aerodynamic changes near and beyond stall. Modern aerofoil design methods seek to optimise aerofoil geometry to obtain the best compromise in performance over the range of design conditions.

Over the past decade, a large number of researchers have investigated the potential for enhancing the performance and behaviour of helicopter rotors by the application of so called "smart" rotor technology. The main aim of smart rotor research

[1]Presented at the 26th European Rotorcraft Forum, The Hague, Netherlands, 26~29 September 2000.

has been to incorporate various forms of smart sensing and controls into the main rotor for the application in vibration and noise reduction, performance enhancement and even as primary controls. There are already ample reviews in this area of research, for example, Friedmann [1], Straub [2] and Chopra [3].

Most researchers consider smart materials e.g. piezoelectric, electrostrictive or magnetostrictive, as embedded actuators to actively twist the rotor to control vibrations. This smart rotor technology falls into the category of active twist rotor or ATR. However currently there are limitations to the range of twist that these actuators can generate. Other researchers have also considered the use of more conventional mechanically actuated flap to overcome the limitation of adaptive material such that a large range of flap deflection can be attained. This falls into the category of active control flap or ACF. Examples of these "smart" rotors are shown in Figure 1 [2,4]. Thus the definition of smart rotor technology has become imprecise and entangled with active control and it is difficult to distinguish the two.

An excellent review of smart rotor research was also provided by Copland [5] where he concludes that due to the limitation of adaptive structure on an actuated scaled rotor, the mechanically actuated flap will possibly offer the best practical application of a flap. A flap positioned at or aft of the trailing edge can be used in a number of different ways to accomplish the three main goals of primary control, vibration reduction and performance improvements. The flap will generate changes in lift, drag and moment in all cases. A flap positioned well aft of the trailing edge is capable of twisting the blade (pitching moment control). However a plain trailing edge flap on a torsionally stiff blade will give increased lift which could provide a performance benefit (lift or camber control). To accomplish certain levels of pitch control it is also usual to reduce torsional stiffness of the blade.

Trailing edge flaps can be externally mounted aft of the trailing edge of the blade as a slotted flap, or as plain flaps which are integrated with the blade profile. By eliminating the hinge gap and flap support structure, plain flaps offer the advantage of reduced power losses due to aerodynamic drag and improved flap effectiveness. To take advantage of the characteristics of plain flaps, the flap actuator and linkage must be small enough to fit within the blade structure. In this study it is assumed that it is possible to incorporate the flap control system within the blade itself, particularly by the application of a servo-actuator. Examples of different types of trailing edge flap are shown in Figure 2 [6,7].

Whilst much effort has been spent in attempting to reduce vibration, the application of smart rotors to increase performance directly is not as well investigated in comparison to vibration reduction. In this paper an analytical evaluation of the Performance Enhancement of the Flap, known henceforth as PEF, will be investigated using the Coupled Rotor Fuselage Model (CRFM), a brief description of its main features will be given. The basic principle of aerodynamic improvement derived from the flap will be discussed. This is followed by a theoretical evaluation of the PEF to a Lynx aircraft to expand its flight envelope and conclusions from this study will be drawn.

2. Brief Description of The Coupled Rotor-Fuselage Model

The CRFM is a comprehensive rotorcraft analysis package capable of predicting aircraft performance, rotor loads, rotor stability and aircraft vibration, in both steady level and manoeuvring flight conditions (Figure 3). The analysis is written to accommodate a wide range of rotorcraft configurations and to include the effects of hub motion due to rigid body and flexible fuselage response. The CRFM is developed jointly by the Defence Evaluation and Research Agency (DERA) of Farnborough and GKN Westland Helicopters Limited (GWHL) in the UK.

The CRFM comprises a dynamic rotor and fuselage representation, unsteady rotor aerodynamics, quasi-steady fuselage aerodynamics, AFCS control laws and a pilot simulation model. The model is constructed so that the complexity of modelling of each component can be chosen to suit the application. Both the aircraft flight mechanics and blade structural loads are calculated at each time step throughout the manoeuvre. The data obtained can then be compared directly with test data as time histories. The essential features and initial application of CRFM can be found in [8] but a summary is provided in the subsequent sections.

In CRFM the fuselage dynamics are described by a general set of modes, typically consisting of the six rigid body modes with optional additional flexible modes. The rotor can be represented as a simple disc model or as a multi-blade dynamic model, where each blade is represented by hub-fixed coupled blade modes, typically comprising 4 flap, 3 lag and 1 torsion mode. The dynamic coupling between the rotor and fuselage is carried out using the branch mode method which links the rotor and

fuselage with a position-fixed rotor centreline and fuselage hub boundary condition implicit in the equation formulation. Transmission or rotor speed freedoms and control circuit dynamics can also be modelled.

In order to allow a single equation to deal with both rigid body and flexible modes, all fuselage forcings (aerodynamic and dynamic) are implemented as modal forcing components applied at the appropriate forcing points. The system dynamic equations in CRFM are written in modal form with a fully flexible definition, allowing the full coupled rotor-fuselage, or either, the rotor or fuselage in isolation to be modelled.

The fuselage aerodynamics are provided as look-up tables from wind-tunnel measurements in terms of local fuselage incidence and sideslip angles. The blade aerodynamics are based on a lifting-line theory for a multiple aerofoil section blade. The blade aerodynamic model includes effects of tip sweep and a simple representation of the yawed flow effect on dynamic stall. The unsteady aerodynamics are represented by an indicial model incorporating a time-delay method for dynamic stall based on the leading edge separation model based on Beddoes [9]. The effects of the PEF model will be included in the indicial model, which will be described later.

CRFM has a number of prescribed wake models including uniform downwash, Glauert, vortex ring, interactive near wake and a wake model suitable for manoeuvre simulation. For this study, the vortex ring wake coupled with the interactive near wake was used. The wake model has been implemented in CRFM such that the wake effects are updated at each azimuth cycle to reflect the changing aircraft state through a manoeuvre.

The pilot simulation model used in CRFM is based on HELMSMAN developed by Hamm [10]. It uses a sophisticated simulation of a helicopter pilot to generate the control inputs required to "fly" the vehicle model through a manoeuvre. The piloting logic uses feedback control algorithms to minimise the difference between the required and the achieved values of selected control parameters, e.g. vertical velocity, bank angle or ground position, so as to accomplish the specified piloting task. Complex manoeuvres, such as transitions and wind-up turns, are flown by switching the piloting aims as intermediate goals are achieved. This mimics the process of a human pilot who, for example on takeoff, uses the collective lever to hold height until a specified speed is achieved and then switches his piloting strategy by adjusting the controls to set and hold the required climb power.

An Automatic Flight Control System (AFCS) was also included to carry out the same functions as on the actual aircraft, e.g. suppression of air resonance and modification of handling qualities. Different forms of AFCS, e.g. simple rate gains, more detailed generic forms and specific proprietary control laws, have been included to enable specific applications.

CRFM produces a timewise solution to the equations of motion using a 4th order Runge-Kutta method. Blade structural loads are calculated using a modal summation method for its simplicity. However a unified formulation method can be applied to account for the local damper load effects in the flatwise and edgewise loads and for the control loads and blade torque arising from higher mode torsional loadings from distributed aerofoils. In addition, an option to calculate blade structural loads using a force integration method based on the Chebyshev polynomial integration has also been developed.

In summary, CRFM has a wide range of comprehensive modelling options for both rotor and vehicle dynamics and aerodynamics. These options provide the fidelity of rotor and vehicle models needed for a comprehensive aeroelastic code. The model is not only capable of performing initial and fast assessment of manoeuvre simulation using a rotor disc model, but it is also capable of loads analysis in level trim and manoeuvre flight when the rotor is modelled as a dynamic multi-blade system. The result of simulating a moderately severe symmetric pull-up manoeuvre as shown in [8] has established CRFM as a tool capable of simulating manoeuvres with timewise histories of aircraft responses and structural loads generated throughout the manoeuvre.

3. Aerodynamic Modelling of Performance Enhancement Flap

3.1 Basic Representation

Dynamic stall adversely affects the aerodynamic performance of a helicopter rotor blade, retreating blade stall being one of the limitations on high speed forward flight of a helicopter. The high transient loads associated with dynamic stall may also induce vibration problems and control system fatigue loads. Alleviation of these effects will expand the flight envelope of the helicopter by reducing the vibratory loads induced by aerodynamic separation and stall.

The main purpose of an active flap is to provide an effective aerofoil camber around the azimuth, thus

modifying the sectional aerodynamic characteristics. The change in camber results in increased lift and also delays the onset of the retreating blade stall. To illustrate the potential benefit from PEF, Figure 4 shows the simplified pitching moment variation around the azimuth of a typical rotor aerofoil at 80%R with and without the flap. The flap is of full span, 10%c and the condition is in high speed forward flight at an advance ratio of μ=0.4. Assuming the pitching moment coefficient to be of constant value, the response for the case without flap is a mainly first harmonic response. In practice, ignoring unsteady effects, the moment coefficient will tend to become more negative (nose-down) on the advancing blade and less negative as the angle of attack increases on the retreating blade, due to separation and Mach number effects. It is observed that the peak pitching moment occurs on the advancing blade at ψ=90°, whilst the moment on the retreating blade at ψ=270° is relatively small due to the large difference in the dynamic head.

If the basic nose down pitching moment coefficient of the unmodified aerofoil is countered by upward deflection of a flap on the advancing side as shown by the dashed line, then the peak pitching moment can be dramatically reduced. A consequent increase in pitching moment on the retreating blade will be of little consequence because of the low dynamic head. For the case with a flap, it is evident that the peak-to-peak pitching moment, and hence control load, has been reduced by two thirds if a flap is actuated as an inverted 1R sine wave of 0°±5° (+ve down). However the flap deflection strategy can be improved further by introducing a mean flap deflection of 3 deg i.e. actuation of 3°±5° as shown in Figure 4. The mean deflection assures a large increase in lift on the retreating side although the mean pitching moment is slightly more negative due to the 3° offset. This will produce a best compromise in terms of overall performance improvement.

Figure 5 shows the aerodynamic characteristics of the same 2D aerofoil with a 10%c flap with deflections of 8°, 3°, 0° and -2° at Mach numbers of 0.3, 0.5 & 0.7, which correspond to a first harmonic actuation of 3°±5° as considered above. It is shown that a 7.5% drag reduction at zero lift coefficient can be achieved at M=0.7 (advancing side) and an increased lift capability of almost 19% was also attained at M=0.3 (retreating side). Also at M=0.5 (both the fore and aft sectors), a 4% improvement was seen in lift together with an improvement in the lift-drag ratio. It is assumed throughout this initial assessment that the addition of a flap had made no difference to the stiffness or dynamic response of the blade.

3.2 Aerodynamic Representation of the Trailing Edge Flap in CRFM

On the basis of these aerodynamic benefits of a flapped aerofoil, the following approach was adopted to assess the benefits of PEF. The method of representing the overall effect on the aerofoil due to the flap deflection is based on the superposition of the thin-aerofoil theory of the indicial unsteady aerodynamic model. The deflection of the flap produces an effective camber which modifies the zero-lift angle (α_0) and the moment coefficient at zero angle of attack (C_{M0}). The changes, $\Delta\alpha_0$ and ΔC_{M0}, which are functions of flap deflection are then fed into the indicial unsteady aerodynamics model. If c_F is the chord fraction of the flap and δ is the flap deflection angle (+ve down, in radians), the effects of a flap model can be described as follows. Using the transformation, $\theta=\cos^{-1}(2c-1)$, then the changes of aerofoil coefficients can be described by;

$$\Delta C_L = 2\delta f_c(\pi + \sin\theta - \theta)\cdot where\cdot f_c = 0.6\cdot for\cdot a\cdot typical\cdot rotor\cdot aerofoil;$$

$$\Delta\alpha_0 = \frac{-\Delta C_L}{2\pi} = \frac{-2\delta f_c(\pi+\sin\theta-\theta)}{2\pi} = \delta f_c\left(1+\frac{\sin\theta-\theta}{\pi}\right)$$

$$\Delta C_{M0} = 0.5\delta f_c \sin\theta(\cos\theta - 1).$$

Both $\Delta\alpha_0$ and ΔC_{M0} can then be used to modify the α_0 and C_{M0} input to unsteady aerodynamic model as a function of flap deflection. The resulting indicial model gives a valid estimate of the overall unsteady behaviour of the flapped aerofoil, including frequency effects on response amplitude and phase. It also enables the changes in performance and vibratory loads to be predicted and so identifies any significant improvement or degradation in the use of smart actuated flap.

3.3 Initial Assessment using CRFM

Having incorporated the aforementioned aerodynamic effects in CRFM, a number of test cases were undertaken to validate the flap model. The potential benefits of deploying the flap can best be illustrated by its effectiveness of delaying the rotor entry into stall. In order to provide an initial assessment, the effect of a PEF on a stalled condition of a Lynx aircraft at 128.9kts, identified in [11], was examined using CRFM, modelled with the full aircraft with the following flap configurations;

no flap;
full span flap (30%R ~ 100%R); and
10% span flap (87%R~97%R)

These cases were chosen to provide a set of datum cases before parametric variations of the flap were carried out. The 10% span flap was selected as a realistic flap configuration as most of the benefits

derived from the flap were expected to be near the blade tip. Both flap cases were for a 10% chord and the flap actuation was an inverted 1R sine wave of 2°±3°. In order to assess the performance benefits from the flap, the flight condition must be of comparable state. Being at the edge of the flight envelope, attempting to "fly" CRFM onto the stalled condition was found to be not straightforward. This reflects that a fully trimmed up aircraft state does not exist when the rotor is stalled. The approach is to fly the aircraft to a lower speed, in this case 50kts, then fly gradually onto the required speed of 128.9kts. This is similar to the pilot's approach. The final simulation cases were started from the same condition without the flap to ensure a common starting point with the aircraft flying onto the trim represented by zero aircraft accelerations.

One of the differences on the trimming philosophy between a simulation and isolated rotor calculation, such as R150 [11], is that the "trim" defined for the latter is based on a cycle-to-cycle repetitiveness. The CRFM assumes "trim" is achieved when the aircraft is in force equilibrium, i.e. zero aircraft accelerations and is more representative than the isolated rotor trim. Figure 6 shows the typical time histories of pitch and roll attitudes for the 3 configurations considered and it is clear that a truly steady state cannot be achieved. Although the difference is numerically small, this can affect the comparisons of the predicted benefit from the PEF.

In order to ensure that the benefits from the flap are not masked by the lack of a cycle-to-cycle trim, it was decided to use the isolated rotor option within CRFM instead of the full aircraft model. Whilst this does not allow a full evaluation of the handling qualities, it provides a quantifiable representation of the performance benefits from the flap. In addition, the number of blade modes has also been reduced to consist of fundamental flap and torsion modes only. This enables the aerodynamic benefits to be assessed independently, reducing the effect introduced by the higher order modes.

One of the main concerns with flap deployment is to ensure that it has no adverse effect on the pilot's control inputs to trim to a particular flight condition. Figure 7 shows the cyclic stick movements against speed. It is evident that there is no deterioration in the F/A cyclic (B1), in fact there is a slight improvement in the control gradient. The results, though not totally conclusive, do indicate that a rotor-fuselage model such as CRFM is needed to investigate the flap model and its effect on handling qualities.

In order to assess the potential benefits of the PEF in delaying entry into the stall , the following definition of the stall boundary is used. The stall boundary is defined by comparing the vibratory (half peak-to-peak) control load (CL_{VIB}) against the monitor level, set at 600lbf, where the case is said to be stalled if CL_{VIB} > 600lbf, as illustrated in Figure 8. Based on this criterion, Figure 9 shows the control load waveform and with the CL_{VIB} for the 3 cases described above. It is evident that the case with 10% span flap reduces the CL_{VIB} by almost 20%.

4. Application of the Performance Enhancement Flap to a Lynx Aircraft

4.1 Parametric Variations of the Performance Enhancement Flap

Having established a suitable analytical model, parametric variations of the flap dimensions were then considered. The parameters investigated included flap spanwise extent, position, chord, deflection amplitude and actuation phasing. The purpose of the study was to identify the most effective combination of the parameters that could be embodied within the various design constraints. These constraints include limitations on flap spanwise extent arising from manufacturing considerations and restrictions on flap chord and deflection due to limitations on actuator force/stroke capabilities. Effects of blade torsional stiffness and control circuit stiffness were also briefly examined. At this stage, the actuation remains as a 1R variation for performance evaluation only and no attempt was made to include higher frequency of actuation for vibration reduction. Based on the datum condition, an optimal flap configuration was derived for a flap centred at 81.4% with a 10.6% span, 20%c and a flap deflection of 4°±5°.

4.2 Application to a Lynx Aircraft with Metal Blades

Using this optimal configuration of the PEF, a range of speed cases was run with and without flap. Figure 10 shows CL_{VIB} v Speed and it is evident that this flap configuration provides an extra 20kts speed capability at the monitor limit. In terms of power saving, it is found to be some 10% at 140kts.

In order to provide an insight into the aerodynamic behaviour, the C_L C_D and C_M for 3 radial stations at 73%, 82% and 88%R, corresponding to radial locations inboard of, on and outboard of the flap spanwise position, are shown in Figure 11. The speed chosen is 140kts at which the conventional

blade is deep into stall on the retreating side. The following points are observed.

The lift coefficient at the inboard station is little affected by the presence of the flap as would be expected since the same trim is maintained. On the flap station it can be seen that whilst the effective incidence has reduced, through deployment of the flap, the lift coefficient has increased, reflecting the increased camber of the aerofoil with the flap. Outboard of the flap station the lift coefficient for the flapped blade exhibits the same trend as that for the baseline blade except that it is smoother in nature.

The curves for drag coefficient also indicate a significant variation with the flap deployment. The drag coefficient reduction is brought about by avoidance of stall in the flapped case. Inboard of the flap the magnitude of the drag coefficient is little changed, but the onset of the first peak of drag coefficient is delayed brought on by the deployment of the flap. Over the span of the flap, the drag rise on the retreating side is virtually eliminated. This is echoed to a lesser extent, outboard of the flap. These results are confirmed by the 10% reduction on the overall profile power for the same trim achieved.

The pitching moment coefficient at all three radial stations for the baseline blade are characterised by a sharp break on the retreating side of the disc indicating stall, followed by oscillations indicative of the blade dynamic response. This behaviour is eliminated with the introduction of the flap at both the flap and the outboard station. Inboard of the flap the behaviour is unchanged except for a delay in the onset of the break.

Figure 12 also shows the integrated aerodynamic root pitching moment and control loads. It can be concluded that the PEF has a considerable effect on the aerodynamic pitching moment due to the change of sectional characteristics as expected even if it only covers 10% of the span. In particular the sudden break in the aerodynamic moment between 180 and 270 azimuth and the subsequent oscillations are suppressed. As suggested before, deployment of the flap allows the blade to be operated at a lower pitch, delaying the onset and reducing the severity of stall at other locations along the blade, especially outboard of the flap.

In order to provide preliminary design information for flap and actuator sizing, the flap hinge load calculation has also been introduced into CRFM. The flap position used was the optimum found from the previous study. A flap deflection of 4°±5° was used while the chord was varied from 10% through 15% to 20%. The results confirm that the hinge moment varies approximately with the square of the chord as would be expected from simple aerodynamic theory and is not excessive.

4.3 Application to a Lynx Aircraft with BERP Blades

Having established theoretically the benefit of a flap on a Lynx aircraft fitted with rectangular blades, the optimal flap configuration was then applied to a Lynx aircraft fitted with BERP blades at a disc loading ($W/\sigma N^2$) of 18000lbf. The flap extent is 76-86.6%R and chord of 20% with a flap deflection of 4°±5°. As the application proceeded it was revealed that the BERP blade first encountered stall at a position some distance inboard of the BERP notch. Consequently an alternative span position of 66-76%R, inboard of the notch was investigated in addition to the original spanwise location. From this study it was evident that the more inboard location offered greater relief of retreating blade stall. Consequently both flap positions were retained for investigation across the complete speed range. The 66-76% R flap was termed Flap1, while Flap 2 had the 76%-86.6% R position.

CRFM was run for a range speeds, both with and without flaps. Control loads and total power consumption were recorded and plotted for each case. The control load waveform was also extracted from the CRFM output and plotted. The predicted waveforms were analysed for their harmonic content. The changes in each harmonic brought about by the introduction of the flap onto the baseline blade were calculated and plotted.

Figure 13 shows the effect of the Flaps-1 and 2 on the vibratory control loads and aircraft power v speed. These results clearly indicate that the introduction of a flap proves beneficial at higher disc loading. While it would be inadvisable to quote any reductions in control loads or total power the plots do indicate that Flap 1 is more effective than Flap 2 at the upper end of the speed range with a 20kts improvement. Figure 14 shows the contour of α-α_0 for the 3 configurations, it is clear that stall region is smaller for Flap 2 compared to Flap 1.

Figure 15 shows the integrated aerodynamic pitching moment and control load waveforms for the 89kts case. From the waveform plots, it can be seen that the flaps are effective in reducing the magnitude of the oscillations apparent in the baseline data, which begin in the vicinity of 270° azimuth and propagate around through 0° to 90° azimuth. This behaviour was apparent from the

previous metal blade study and indicates that the flap is most effective when the rotor is highly loaded near the extremities of the operating envelope.

Harmonic analyses of the effectiveness of the flaps are also presented in Figure 16. For these plots the control load waveforms for the baseline and flap cases were decomposed into their harmonic components. The changes in each harmonic brought about by the introduction of the flap into the baseline blade were calculated and plotted in a histogram format. Each harmonic was expressed in its cosine component (A), sine component (B) and its vector magnitude (C). The result indicates that the higher harmonics are generally more heavily affected than the lower orders. For both flaps the 5R and 6R harmonics appear to be changed the most on average across the speed range. This is probably due to the flap suppressing the oscillations of the blade brought about when encountering stall on the retreating side of the disc.

5. Conclusions

A numerical evaluation of the potential benefits of an actuated trailing edge flap has been presented. The principles giving rise to the aerodynamic benefits have been described and were introduced into the Coupled Rotor-Fuselage Model. The Performance Enhancement Flap (PEF) is found to be most effective in suppressing retreating blade stall, and hence offers an expansion of the flight envelope.

Although this study indicates the potential benefits, a considerable amount of work is still required on structural modelling, dynamics, aeroelastics, aerodynamics, materials and control of these devices before a flap can be implemented on a full-scale helicopter in flight. Also handling characteristics will need further scrutinisation, but to-date the computed stick gradients were favourable.

In addition, further work is needed to design a practical actuation mechanism. Actuation devices have not yet matured beyond a preliminary stage and so the potential of the flap is yet to be fully proven. Significant research needs to be undertaken into the implementation of such devices in the rotorcraft environment.

The effects of the performance enhancement flap were theoretically demonstrated on a Lynx aircraft with both metal and BERP blades. The quantitative benefits using the PEF are shown to be capable of expanding the flight envelope by some 20kts.

Acknowledgements

This programme of study was funded by the United Kingdom Ministry of Defence (Procurement Executive), under the contractual supervision of Aircraft System Division of DERA (Farnborough), UK.

The authors would also like to acknowledge the contributions from our colleagues D Jessop and D Bowhay of GKN Westland Helicopters Limited and Dr R Markiewics and I Kaynes of DERA, Farnborough.

References

1. Friedmann P.P., “The Promise of Adaptive Material for Alleviating Aeroelastic Problems and Some Concerns”, RAeS Proceedings on “Innovation in Rotorcraft Technology”, London 24~25 June 1997

2. Straub F.K., “Active Flap Control for Vibration Reduction and Performance Improvement”, Paper Presented at the AHS 51st Annual Forum, Texas, May 1995

3. Chopra I., “Application of Smart Structures Technology to Rotorcraft Systems”, Journal of Smart Material Structures, Vol.5, No.1 February 1996

4. Chen P.C. & Chopra I., “Hover Testing of Smart Rotor with Induced-Strain Actuation of Blade Twist”, AIAA Journal Vol.35, No.1, January 1997

5. Copland C., “A Review of Smart Rotor Technology, Unpublished DERA Report, June 1998

6. Straub F.K. & Hassan A.A., “Aeromechanic Considerations in the Design of a Rotor with Smart Material Actuated Trailing Edge Flaps”, Paper presented at the American Helicopter Society 52nd Forum, Washington D.C., June 1996

7. Straub F.K. & Merkley D.J., “Design of a Servo-Flap Rotor for Reduced Control Loads”, Paper presented at the AHS 50th Forum, May 1994

8. Chan W., Holton S.A. and Hamm J.C., “Results of Initial Aircraft Manoeuvre Simulation on the Coupled Rotor-Fuselage Model”, Paper presented at the American Helicopter Society 55th Forum, Montreal, Quebec, Canada, May 1999

9. Beddoes T.S., “Onset of Leading Edge Separation Effects under Dynamic Conditions and Low Mach Numbers”, Paper presented at the

American Helicopter Society 34th Annual Forum, Washington, D.C., May 1978

10. Hamm J.C., "The Development of Helicopter Pilot Models to Control Engineering Simulations", Paper presented at the Royal Aeronautical Society, Conference on Rotorcraft Simulation, 18th May 1994

11. Lau B.H., Louie A.W., Griffiths N. and Sotiriou C.P., "Correlation of The Lynx-XZ170 Flight Test Results Up To and Beyond The Stall Boundary" Paper presented at the American Helicopter Society 49th Annual Forum, St Louis, Missouri, May 1993

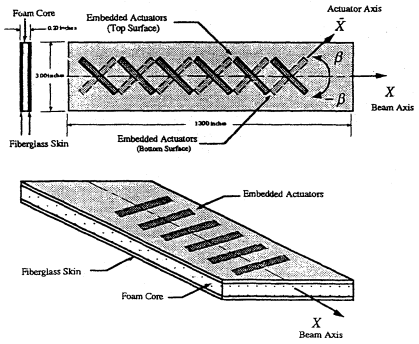

a) Active twist rotor using embedded piezoelectric torsional actuators (from Chen & Chopra, ref. 4)

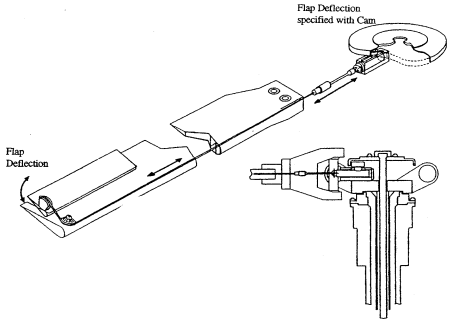

b) Active control flap using a cam-driven mechanism (from Straub, ref. 2)

Figure 1: Example of a "smart" rotor

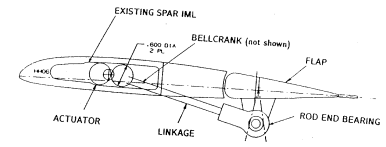

a) Flap

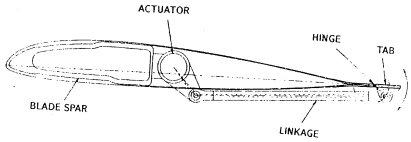

b) Tab

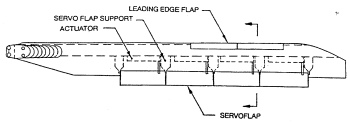

c) Trailing edge flap (Externally mounted)

Figure 2: Example trailing edge flaps (from Straub *et al.*, ref. 6,7)

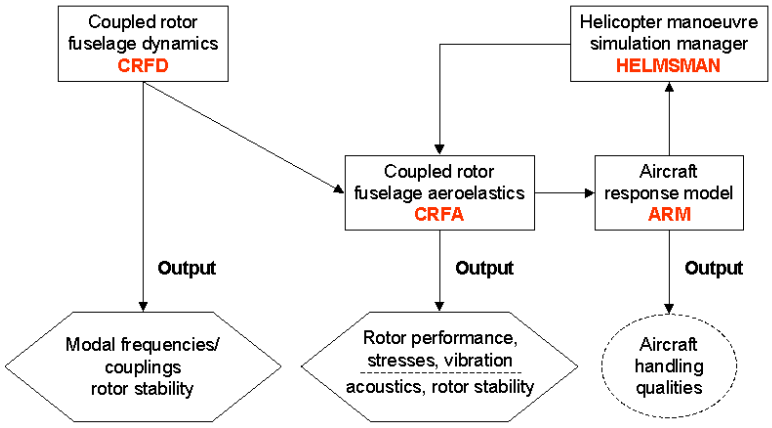

Figure 3: The Coupled Rotor Fuselage Model (CRFM)

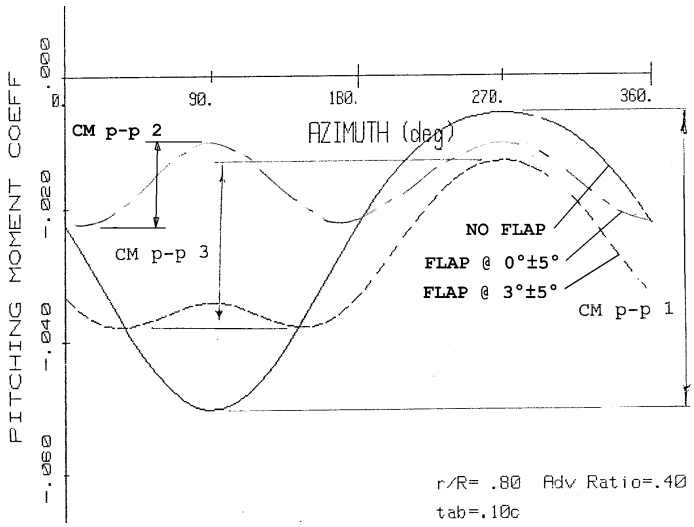

Figure 4: Pitching moment variations

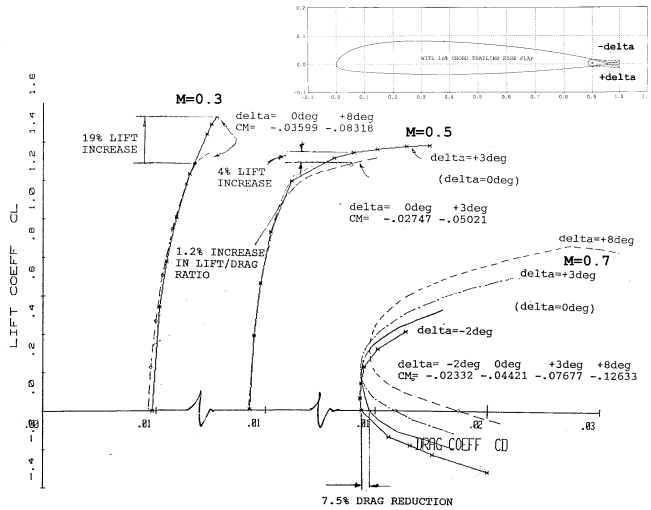

Figure 5: Aerofoil characteristics at different Mach numbers

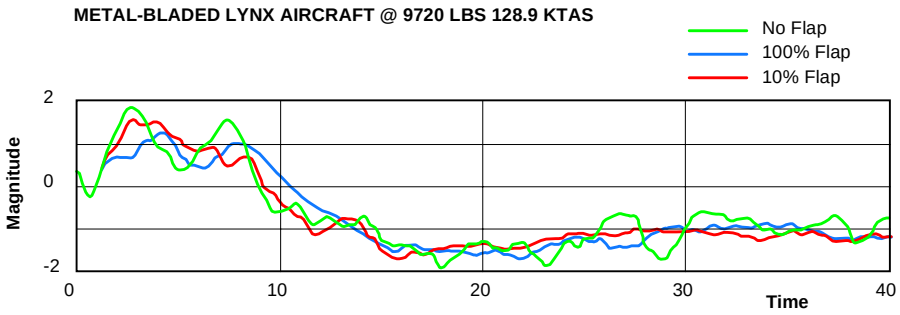

Figure 6: Pitch attitude trace

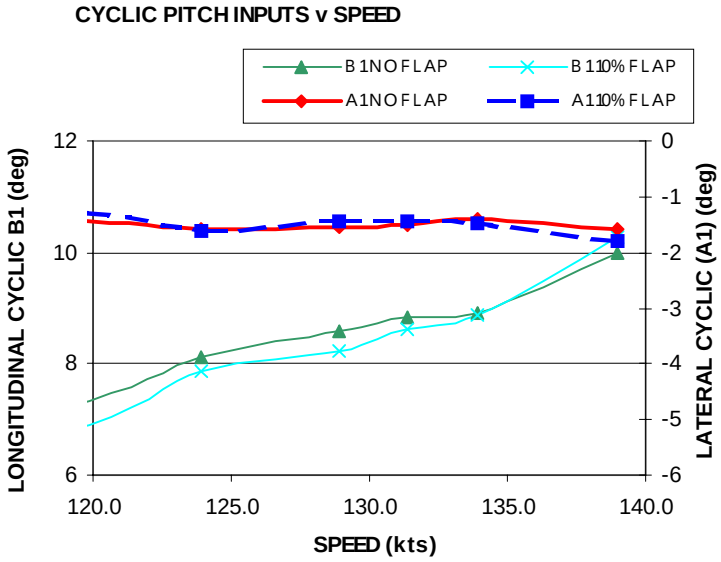

Figure 7: Pilot's control variation

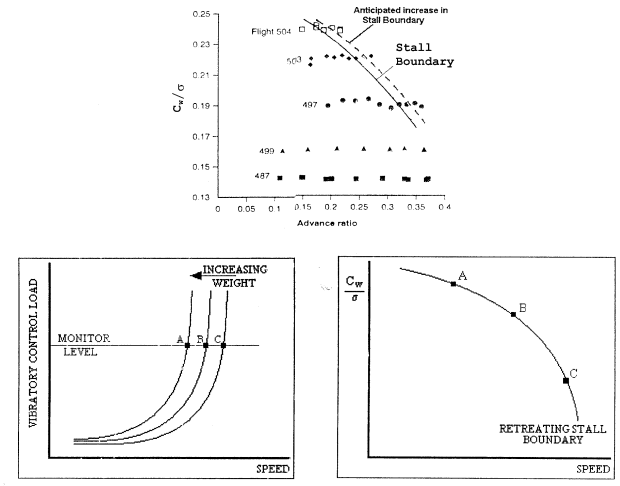

Figure 8: Definition of stall boundary

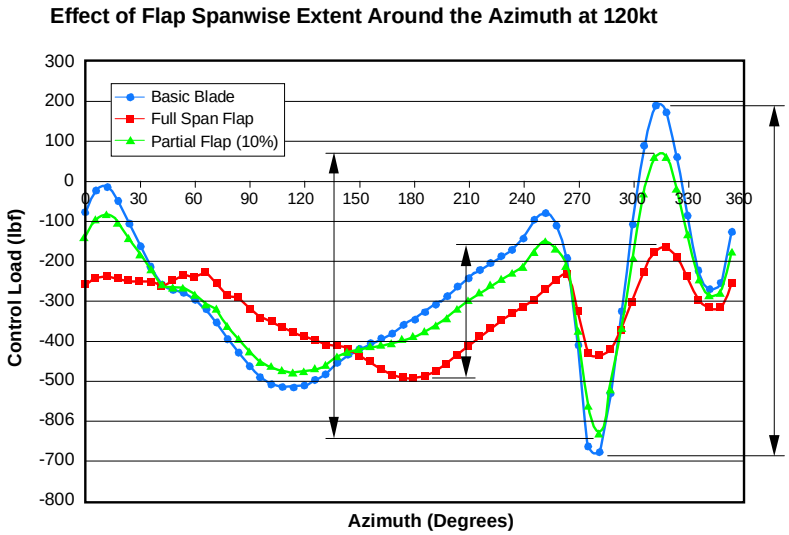

Figure 9: Control load waveform

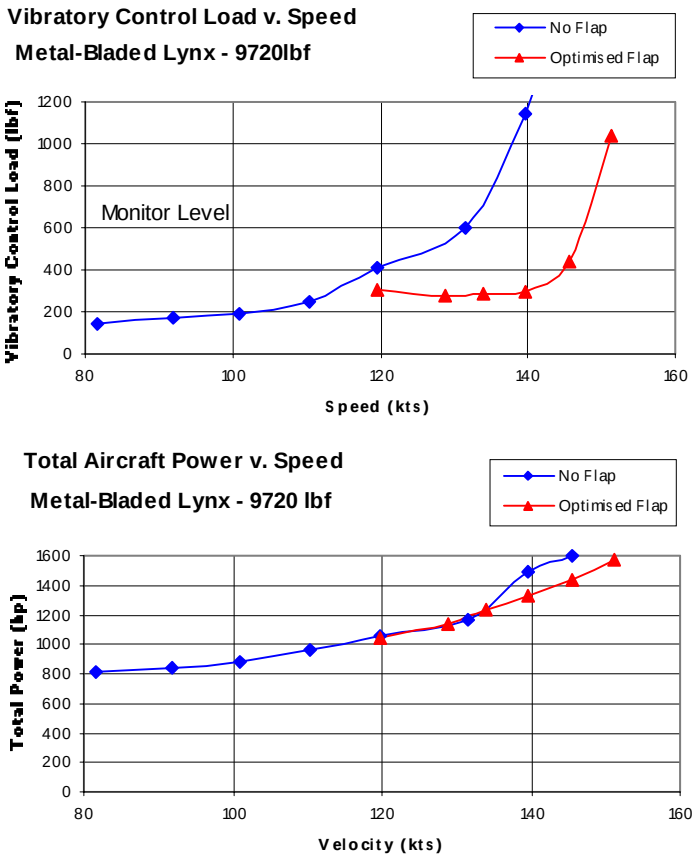

Figure 10: Effect of flap on vibratory control load & power

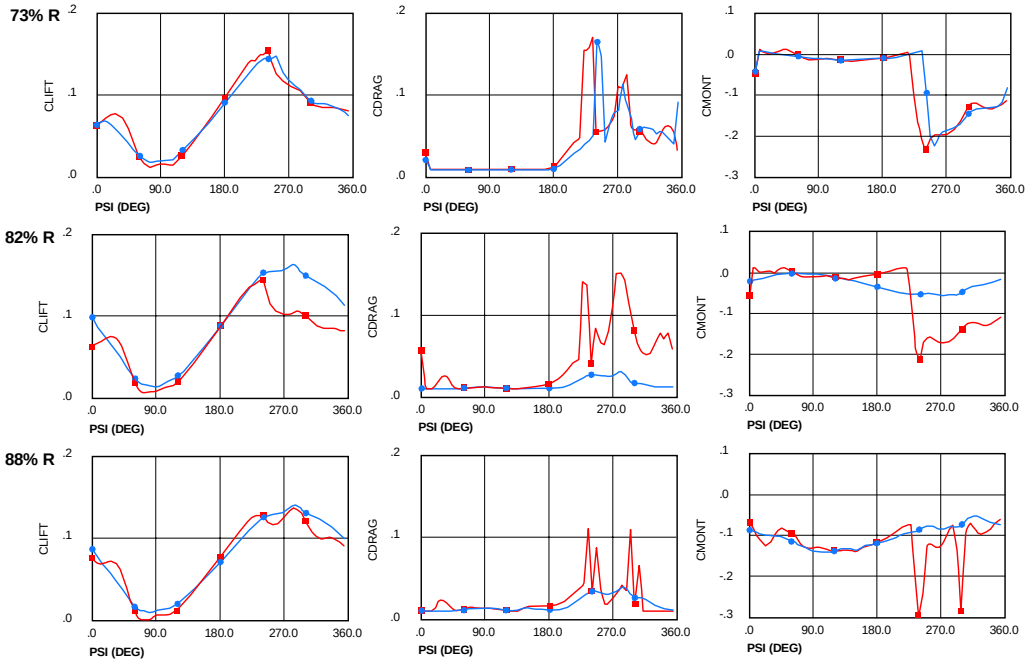

Figure 11: Aerodynamic coefficients for metal-bladed Lynx 139.7 kts

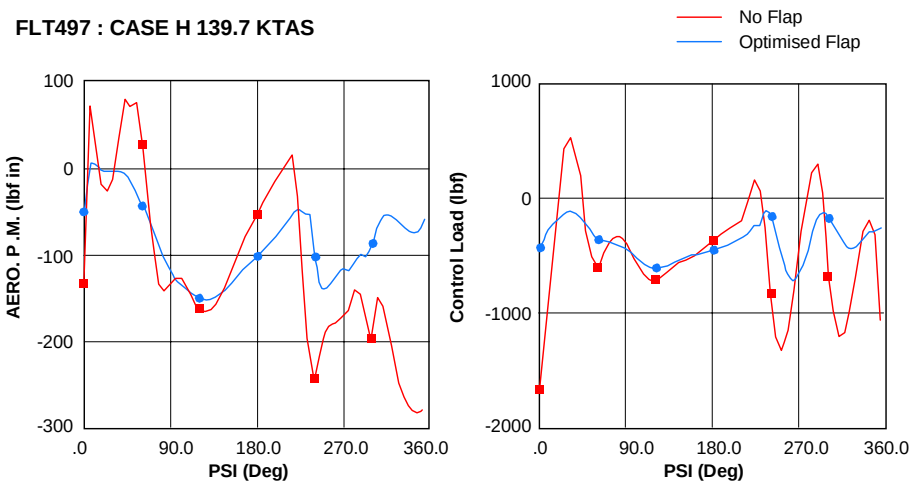

Figure 12: Root aerodynamic pitching moment and control load waveform

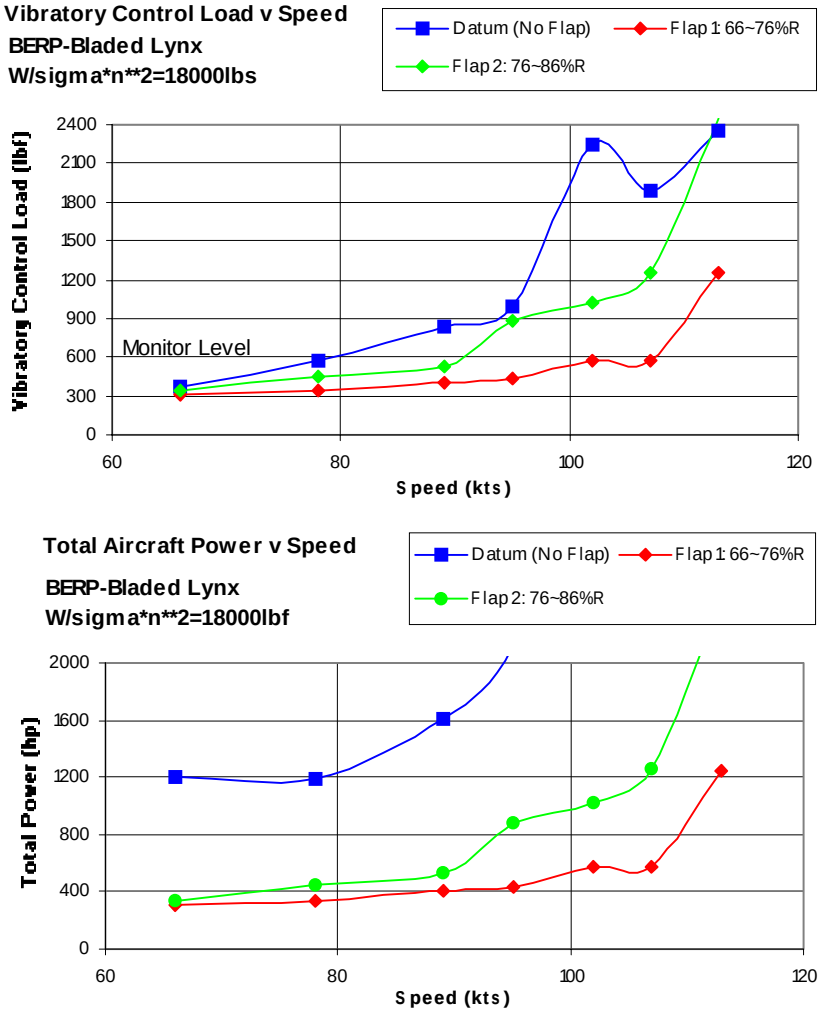

Figure 13: Vibratory control load & total aircraft power versus speed

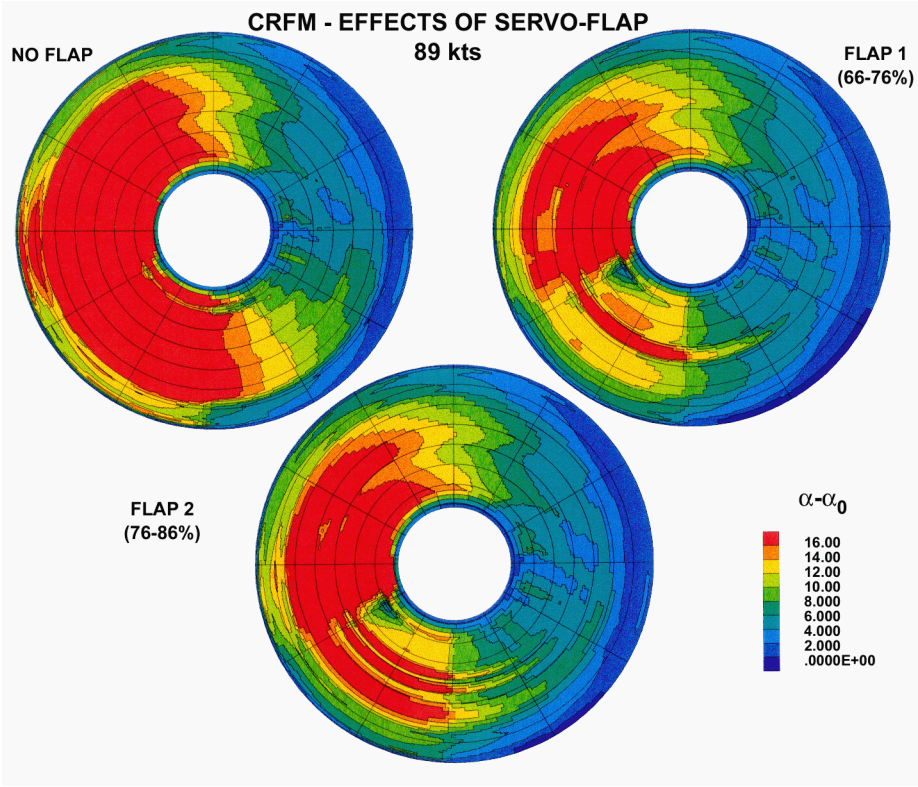

Figure 14: Comparison of α-α_0 for various flap positions

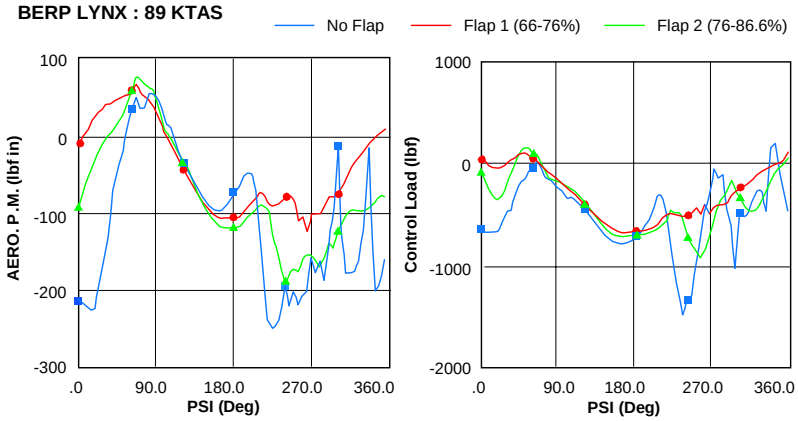

Figure 15: Root aerodynamic pitching moment and control load waveform

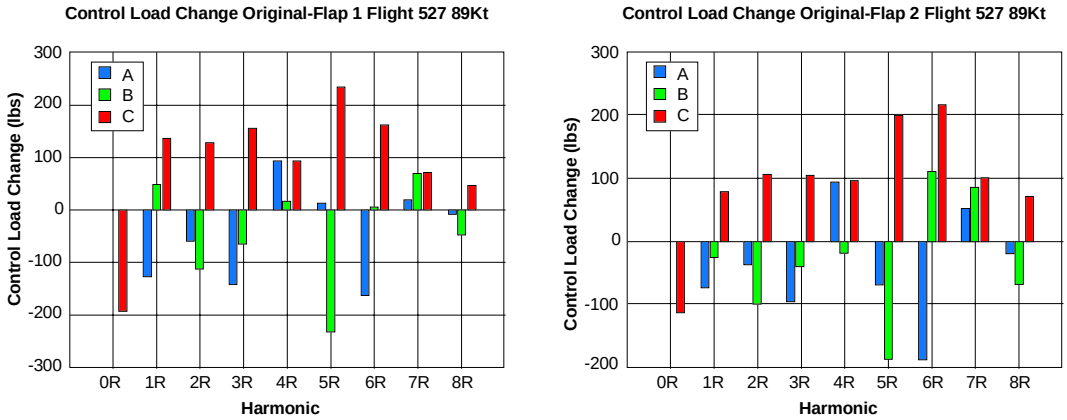

Figure 16: Control load harmonic components versus datum (no flap)